Edge technique: theory and application to the lidar measurement of atmospheric wind

C. Laurence Korb, Bruce M. Gentry, and Chi Y. Weng

The edge technique is a new and powerful method for measuring small frequency shifts. With the edge technique a laser is located on the steep slope of a high-resolution spectral filter, which produces large changes in transmission for small frequency shifts. A differential technique renders the frequency shift measurement insensitive to both laser and filter frequency jitter and drift. The measurement is shown to be insensitive to the laser width and shape for widths that are less than the half-width of the edge filter. The theory of the measurement is given with application to the lidar measurement of wind. The edge technique can be used to measure wind with a lidar by using either the aerosol or molecular backscattered signal. Examples of both measurements are presented. Simulations for a ground-based lidar at 1.06 μm using reasonable instrumental parameters are used to show an accuracy for the vector components of the wind that is better than 0.5 m/s from the ground to an altitude of 20 km for a 100-m vertical resolution and a 100-shot average. For a 20-m vertical resolution and a 10-shot average, simulations show an accuracy of better than 0.2 m/s in the first 2 km and better than 0.5 m/s to 5 km.

1. Introduction

The edge technique is a powerful new method for the detection and measurement of small frequency shifts.[1] This approach lends itself to a variety of applications including the measurement of the Doppler shift to determine the component of the velocity of an object along the line of sight of a laser beam. In particular it can be used with a lidar system to obtain range-resolved measurements of the atmospheric wind.

In the edge technique, the laser frequency is located on the edge of the spectral response function of a high-resolution optical filter. Because of the steep slope of the edge, small changes in frequency, as a result of Doppler shifts, produce large changes in filter transmission. The shift is determined from a differential measurement of the frequency of the outgoing laser beam and the laser return reflected from the target. The resulting measurement is insensitive to laser frequency jitter and drift.

Our primary interest is in utilizing the edge technique with a lidar system for remote measurement of the wind velocity remotely. Recent studies indicate that a global determination of the tropospheric wind field to an accuracy of 1–5 m/s is the single most important measurement for numerical weather forecasting.[2–4] This measurement could be carried out with a spaceborne lidar system that senses the Doppler shift of a laser signal backscattered from the atmosphere. In addition high spatial and temporal resolution wind measurements from ground-based or airborne remote-sensing systems are important in describing the evolution of mesoscale circulations associated with various atmospheric phenomena including deep and shallow convection, density currents, and gravity wave activity. These data would be important for understanding and modeling these phenomena as well as forecasting severe weather events. Such measurements could also be applied to the detection of wind shear, microbursts, and turbulence, which represent significant aircraft safety hazards. The high accuracy and high vertical resolution that can be obtained with the edge technique will provide a capability of directly observing vertical winds, which will permit studies of turbulent motion and the evolution of convective cells in the boundary layer.

Doppler lidars employing heterodyne detection at 10 μm have been used previously for atmospheric wind sensing.[5–7] This technology will be used for the Laser Atmospheric Wind Sounder to be flown on the Earth Observing System.[8–10] For spaceborne applications such a system requires a 10-J/pulse CO_2 laser operating at an isotopic line in the 9–10-μm region. The Laser Atmospheric Wind Sounder instrument

C. L. Korb and B. M. Gentry are with Laboratory for Atmospheres, Code 917, NASA Goddard Space Flight Center, Greenbelt, Maryland 20771; C. Y. Weng is with Science Systems and Applications Inc., Seabrook, Maryland 20706.

Received 13 September 1990.

design panel identified a minimum atmospheric aerosol backscatter coefficient of 1×10^{-10} m^{-1} sr^{-1} for a 1-m/s accuracy.[11] The Global Backscatter Experiment[12] has made aircraft measurements of atmospheric backscatter in a wide range of conditions to determine whether the magnitude of the aerosol backscatter at CO_2 laser wavelengths is sufficient for tropospheric wind measurements over the globe. To obtain increased atmospheric backscatter, lidar systems employing heterodyne detection at shorter wavelengths have been proposed,[13–15] and a system operating at 2.1 μm is under development for ground-based use.[16] The use of incoherent detection with a spatially scanned Fabry–Perot étalon has been proposed also[17–19] and a ground-based system has been used to measure winds.[20] Recently a ground-based lidar using dual Fabry–Perot étalons located on either side of the broadband Rayleigh spectrum has been used to determine winds in the stratosphere by measuring the Doppler shift of the Rayleigh backscattered signal.[21]

The edge technique, using a lidar system, can measure wind velocity with high accuracy and high vertical resolution. The measurement principles can be used at any wavelength. The use of a differential technique to measure the Doppler shift renders the measurement insensitive to laser frequency jitter and drift. The edge measurement is also insensitive to the spectral width of the laser provided the laser width is of the order of or smaller than the half-width at half-height (HWHH) of the edge filter. The frequency measurement accuracy that can be achieved is ~100 times better than the spectral bandwidth, the combined width of the laser and the filter. We have demonstrated these characteristics of the edge technique in laboratory experiments.[22] A very high vertical resolution, i.e., as high as 10 m, can be achieved with the edge technique since the relatively broad laser spectral width allowed by this technique permits the use of a short temporal pulse length. With the edge technique the edge filter is used as a static spectral filter, and a spectral scan is not required as with other incoherent methods.[17–20] As a result, the laser energy may be used at or near the edge filter location that has maximum sensitivity to the Doppler shift. Also, because incoherent detection is used, the field of view of the telescope can be hundreds of times diffraction limited, which permits the transmitted laser beam to have a relatively large divergence. The effects of speckle are minimized since thousands of spatial cells are averaged in each measurement. The energy density of the transmitted laser beam will also be reduced by thousands of times so that short-wavelength, solid-state lasers such as Nd:YAG can be used. A lidar operating at short wavelengths, in the visible to near IR, would obtain orders-of-magnitude larger backscattered signal from the atmosphere than it would at 10 μm.

The theory of edge detection is presented in Section 2. The theory includes a description of the differential frequency measurement and the method of normalizing the measurement for the incoming signal magnitude. The effects of finite laser width are included. The edge technique is shown to be insensitive to the laser spectral width and shape for a broad range of conditions. The methodology for evaluating velocity measurement errors is also given. In Section 3 applications of the edge technique to lidar wind measurement are presented. Two fundamentally different ways of using the edge technique to measure winds are considered in three examples. In the first two examples, at 1.06 and 0.53 μm, a high-resolution filter is utilized to measure the Doppler shift of the aerosol return, and thus the wind, with high sensitivity. The third example shows how the wind may be determined by measuring the average drift component of the molecular velocity by using a lower-resolution edge filter and the large Rayleigh backscattered signal obtained in the UV.

2. Theory

The wind velocity is obtained with a lidar by measuring the Doppler shift caused by the motion of atmospheric backscatterers. A schematic of a lidar system that uses the edge of a spectral filter and a narrow-band laser to measure the Doppler shift is shown in Fig. 1. A small fraction of the laser signal is picked off from the outgoing beam. This signal is split between an edge filter detector (DET 2) and an energy monitor detector (DET 1). A portion of the laser signal transmitted to the atmosphere is backscattered from each range element of the atmosphere, and the resultant signal is collected by a receiver. This signal is also split, as above, between the edge filter and the energy monitor detectors.

The Doppler shift is determined from a differential measurement of the frequency of the outgoing laser pulse and the laser return backscattered from the atmosphere. This is accomplished by measuring the normalized edge filter output (DET 2/DET 1) for both the outgoing and backscattered laser signals on

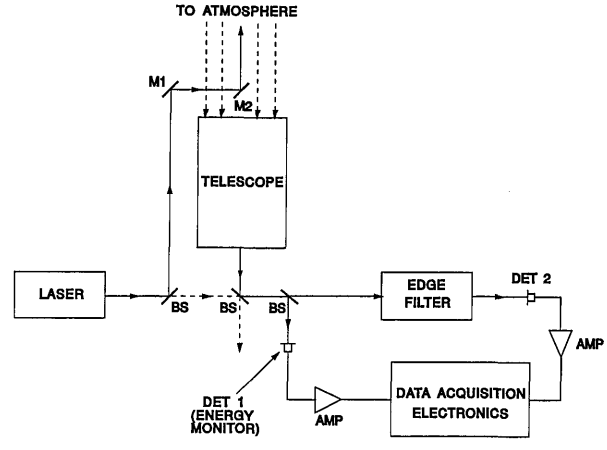

Fig. 1. Block diagram of the optical layout for a lidar when the edge technique is used. The normalized edge signal, the ratio of the detector outputs, is measured for the outgoing and backscattered laser signals for each pulse. BS's, beam splitters; M1, M2, mirrors; AMP's, amplifiers.

a per-pulse basis, taking the difference in these outputs, and utilizing a knowledge of the average slope of the edge in the region of the measurement. Because of the differential nature of the measurement, the result is insensitive to laser frequency jitter and drift. The measurement can be set up for maximum sensitivity by utilizing that region on the edge of the filter transmission profile that has the greatest fractional change in measured signal for a given frequency shift. For a given incident photon flux the minimum measurement error is obtained by optimizing the combined measurement sensitivity and signal to noise.

An edge filter with a sharp spectral response function is required (see Fig. 2). The function is characterized by the central frequency ν_0 and the half-width at half-height α. For a laser centered at frequency ν, the transmission of the edge filter as observed by the laser is

$$F(\nu) = \int_{-\infty}^{\infty} h(\nu - \nu')\, f(\nu')\mathrm{d}\nu' \tag{1}$$

where $h(\nu - \nu')$ is the spectral distribution of the laser energy normalized to have a unit area and $f(\nu')$ is the transmission function of the edge filter. The signal transmitted through the edge filter and measured by a photodetector $I(\nu)$ is given by

$$I(\nu) = GgI_0F(\nu), \tag{2}$$

where I_0 is the incident signal, G is the detector gain, and g is the detector quantum efficiency times the transmission of all optical elements in the edge channel other than the filter. To account for the magnitude of the backscattered signal, an additional detector is used as an energy monitor to measure the intensity of the beam prior to transmission through the filter. Its signal I_{EM} is given as

$$I_{\mathrm{EM}} = G_0g_0I_0, \tag{3}$$

where G_0 is the detector gain and g_0 is the product of the detector quantum efficiency and the optical transmission of the energy monitor channel. The ratio of the signals from the filter and energy monitor detectors gives the normalized signal $I_N(\nu)$ as

$$I_N(\nu) = CF(\nu), \tag{4}$$

where

$$C = \frac{Gg}{G_0g_0}.$$

The constant C can be determined by a calibration measurement.

The Doppler shift is determined from a differential frequency measurement as follows. A small portion of the outgoing laser beam is sampled to determine the normalized signal $I_N(\nu)$, as given in Eq. (4). The laser energy backscattered from the atmosphere is Doppler shifted by an amount $\Delta\nu$. The backscattered signals $I(\nu + \Delta\nu)$ and I_{EM} are measured by the edge and energy monitor detectors, respectively, as before. The normalized signal is found to be

$$I_N(\nu + \Delta\nu) = CF(\nu + \Delta\nu). \tag{5}$$

We note that $I_N(\nu + \Delta\nu)$ is uniquely related to the Doppler-shifted frequency $\nu + \Delta\nu$, provided that $\nu + \Delta\nu > \nu_0$ (see Fig. 2).

The difference in the normalized signals ΔI_N is found by subtracting Eq. (4) from Eq. (5) to obtain

$$\Delta I_N = C[F(\nu + \Delta\nu) - F(\nu)]. \tag{6}$$

The quantity in brackets in Eq. (6) is the change in the transmission of the edge between the outgoing and backscattered measurements, as a result of the Doppler shift, as observed with the laser. The Doppler shift is found from Eq. (6) to be

$$\Delta\nu = \frac{\Delta I_N}{C\beta(\nu, \Delta\nu)}, \tag{7}$$

where

$$\beta(\nu, \Delta\nu) = \frac{F(\nu + \Delta\nu) - F(\nu)}{\Delta\nu}. \tag{8}$$

The physical interpretation of Eq. (8) is that β is the average slope of the edge function as observed with the laser on the finite interval ν to $\nu + \Delta\nu$. An expression for β can be found by using a Taylor series expansion of $F(\nu + \Delta\nu)$ as

$$\beta(\nu, \Delta\nu) = F'(\nu) + F''(\nu)\frac{\Delta\nu}{2} + \cdots, \tag{9}$$

where F' and F'' are the first and second derivatives of $F(\nu)$. The derivative $F'(\nu)$ can be determined by scanning either the laser or the filter over the other element during system calibration. The value of $F'(\nu)$ can be used as an initial value for β in Eq. (7). For small Doppler shifts this is essentially an exact

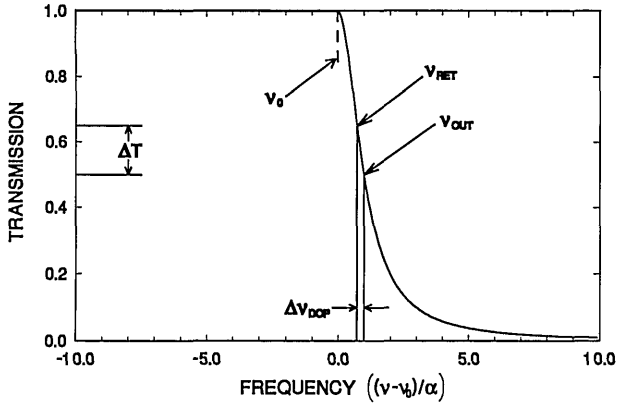

Fig. 2. Spectral response of a high-resolution filter as a function of frequency in units of the filter half-width α. The location of the outgoing and backscattered laser frequencies, ν_{OUT} and ν_{RET}, are shown on the edge of the filter. A small Doppler shift $\Delta\nu_{\mathrm{DOP}}$ produces a large change in signal ΔT.

solution. For large Doppler shifts the shift determined from Eq. (7) can be used iteratively with Eq. (8) to determine β, and thus $\Delta\nu$, to any required accuracy.

Alternatively, the Doppler shift may be found directly from Eqs. (4) and (5). A lookup table, generated by scanning either the laser or the filter over the other element during the system calibration, is used to find the frequency for each of the two measured values of transmission, $F(\nu)$ and $F(\nu + \Delta\nu)$. The Doppler shift is the difference between the two frequencies.

Two important features of the edge technique are the insensitivity of the measurement to the laser spectral width and shape. It is clear from Eq. (7) that the measurement of the Doppler shift will be independent of the laser spectral width and shape if the differential normalized signal ΔI_N and the average slope β are independent of these properties. From Eq. (6) and the definition of F, Eq. (1), it follows that ΔI_N can be expressed as

$$\Delta I_N = C \int_{-\infty}^{\infty} h(\nu - \nu'')[f(\nu'' + \Delta\nu) - f(\nu'')]\mathrm{d}\nu'', \tag{10}$$

where a change of variable, $\nu'' = \nu' - \Delta\nu$, has been made. For the case of an edge measurement where the edge function $f(\nu)$ is linear over the laser width and the region of the measurement, $\nu'' - \Delta\nu_L$ to $\nu'' + \Delta\nu + \Delta\nu_L$ (where $\Delta\nu_L$ is the laser width), the quantity in brackets in Eq. (10) is a constant. Thus the differential normalized signal

$$\Delta I_N = C[f(\nu'' + \Delta\nu) - f(\nu'')] \tag{11}$$

is independent of the laser spectral width and shape. Similarly the average slope β is given as

$$\beta(\nu, \Delta\nu) = \int_{-\infty}^{\infty} h(\nu - \nu'')\left[\frac{f(\nu'' + \Delta\nu) - f(\nu'')}{\Delta\nu}\right]\mathrm{d}\nu''. \tag{12}$$

The term in brackets in Eq. (12) is the slope of $f(\nu)$, which is a constant if $f(\nu)$ satisfies the conditions described above. An expression for β that is analogous to Eq. (11) results. Thus β as well as ΔI_N is independent of the laser spectral width and shape. It follows that if $f(\nu)$ is linear over the laser width and region of measurement, the determination of the Doppler shift $\Delta\nu$ is independent of the laser spectral properties and is equivalent to a measurement with a monochromatic laser. Furthermore, it may be shown that for a laser line shape that is symmetric the edge is required to be linear over only the laser width and not over the Doppler shift. For this case the analysis is valid for large Doppler shifts. In general the theoretical treatment given for the edge technique, beginning with Eq. (1), includes finite laser bandwidth and is not limited in any way by a requirement that the edge be linear over the laser width or the region of the Doppler shift.

Because of the two-way path in a lidar measurement, the backscattered radiation is Doppler shifted twice, that is

$$\Delta\nu = \left(\frac{2v}{c}\right)\nu, \tag{13}$$

where v is the component of the velocity of the wind along the line of sight of the laser and c is the speed of light. The velocity is found from Eqs. (7) and (13) to be

$$v = \frac{c}{2\nu}\frac{\Delta I_N}{C\beta}. \tag{14}$$

We note this equation's similarity in form to Eq. (8) of Ref. 17.

It is useful to define the measurement sensitivity as the fractional change in the normalized measured signal for a unit velocity. The sensitivity is

$$\Theta = \frac{1}{v}\frac{\Delta I_N}{I_N}. \tag{15}$$

The error ϵ in the line-of-sight velocity at a given point on the edge can be computed from the sensitivity by noting that

$$\epsilon = \frac{1}{(S/N)\Theta}, \tag{16a}$$

where (S/N) is the signal-to-noise ratio for the measurement of the differential normalized signal. For a measurement at a zenith angle γ_Z the error in the horizontal component of the velocity is

$$\epsilon_H = \frac{\epsilon}{\sin(\gamma_Z)}. \tag{16b}$$

The error that is due to the signal-to-noise ratio is dominated typically by the error in the atmospheric component of the differential normalized signal measurement. For the case of a moderately high signal-to-noise ratio in both the edge and energy monitor channels, the noise in the measurement may be considered to be uncorrelated, and the composite signal-to-noise ratio is given as

$$\frac{1}{(S/N)} = \left[\frac{1}{(S/N)_1{}^2} + \frac{1}{(S/N)_2{}^2}\right]^{1/2}, \tag{17}$$

where $(S/N)_1$ and $(S/N)_2$ are the signal-to-noise terms for the measurement of the atmospheric backscattered signal by the edge filter and energy monitor detectors, respectively.

3. Applications

A. Introduction

Various techniques and instruments could be used to produce an edge filter with a sharp spectral feature. Some examples include the use of a narrow absorption line, an atomic absorption filter, a spherical or

plane Fabry–Perot étalon, a Fizeau étalon, a grating, or a prism. A variety of laser wavelengths can be utilized since there are no inherent restrictions on the choice of wavelength with the edge technique. The selection of the wavelength is based on the atmospheric backscatter, the transmittance, and the performance characteristics of the laser and detector. It is important to note that the edge technique uses the edge filter as a static spectral filter, which allows the laser energy to be utilized with maximum sensitivity to the Doppler shift. The edge technique does not require a spectral scan as in other incoherent methods.[17–20]

To illustrate the power of the edge technique in a lidar wind measurement, we consider two fundamentally different ways that an edge filter can be used to measure the wind. A high-resolution edge filter may be used to measure the shift of the aerosol return, which has a narrow spectral distribution that is similar to the sharp spectral distribution of the laser. This technique can be used in the near-IR or visible region to achieve high sensitivity. The broadband Rayleigh return for this case will constitute a background that must be compensated for. The second approach is to use a lower-resolution edge filter, whose width is of the order of the Rayleigh width, to measure the shift of the combined Rayleigh and aerosol returns. This method would have reduced sensitivity but would have drastically increased backscattered signal for measurements in the UV. In the following examples the central fringe of a Fabry–Perot étalon is used as the edge filter.

The spectral response of a Fabry–Perot étalon is given by the Airy function.[23] The transmission of the central fringe may be expressed by a Lorentzian[24,25] as

$$f(x) = \frac{1}{1 + x^2}, \tag{18}$$

where $x = (\nu - \nu_0)/\alpha$ and α is the HWHH of the étalon fringe. For measurements on the edge of the étalon fringe where $f(x)$ may be considered to be linear over the width of the laser, the edge measurement may be approximated by a monochromatic measurement, as discussed in the previous section. The fractional change in the normalized signal $\Delta I_N / I_N$ is then equal to the fractional change in f, and the sensitivity [Eq. (15)] is

$$\Theta = -\frac{1}{v}\frac{2x}{1 + x^2}\,dx, \tag{19}$$

where $dx = d\nu/\alpha$. It follows from Eq. (19) that the measurement sensitivity for a unit velocity has a maximum value at the half-width, $x = 1$, of $d\nu/\alpha$.

A more generalized treatment that does not require an assumption of linearity is as follows. For a laser with a finite bandwidth and a spectral distribution $h(\nu)$, the observed transmission is given by Eq. (1) where Eq. (18) is the transmission function of the edge filter. The sensitivity for a laser with a finite spectral width is given in Fig. 3 for various ratios of the laser spectral width [full width at half-height (FWHH)] to the étalon half-width (HWHH) as calculated from Eqs. (1), (15), and (18) for a resolving power $\nu/\Delta\nu$ of 2.8×10^6. The sensitivity is shown as a function of the location of the measurement on the edge in units of fringe half-widths. The simulations are for a Gaussian laser line shape. For example, the solid curve shows the sensitivity for a monochromatic laser. We note that this result could also be obtained from Eq. (19). The sensitivity is defined as the fractional (or percentage) change in signal for a velocity of 1 m/s. In Fig. 3 we see that the peak sensitivity of nearly 4% change in signal for a velocity of 1 m/s is obtained near the half-width. The physical significance of the sensitivity may be seen by considering that if a 1% measurement of the differential normalized signal is made, the corresponding velocity accuracy is 25 cm/s. We believe that wind measurements to accuracies of better than 25 cm/s should be possible since we have made lidar measurements of atmospheric transmission to accuracies of better than 0.5% in differential absorption lidar measurements of the atmospheric pressure profile (pressure accuracy of 0.1%–0.2%).[26] As shown in Fig. 3 the finite laser width affects the sensitivity for measurements located less than one laser width, FWHH, from the center frequency of the fringe. Although the sensitivity is reduced in this region, accurate measurements are still obtained. At locations that are further out on the edge the sensitivity is largely unchanged.

The atmospheric backscattered signal for channel i, the edge filter or energy monitor path through the system, is found as follows. For a lidar with a coincident transmitter and receiver operating at a wavelength λ with a pulse energy E_0, the number of photons detected in channel i from an element of the

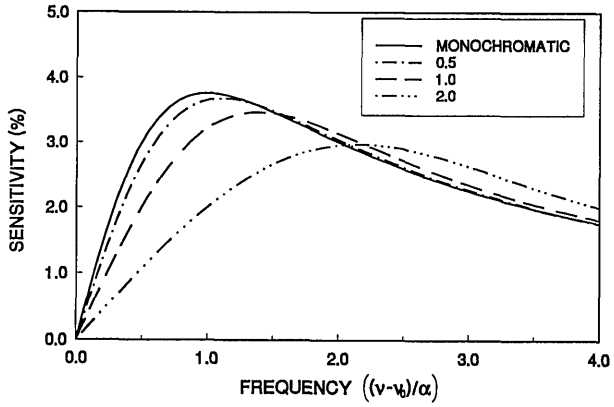

Fig. 3. Sensitivity, the percentage change in the differential normalized edge signal for a velocity of 1 m/s, plotted as a function of the location of the measurement on the edge in units of fringe half-widths. The curves are shown for different ratios of the laser spectral width (FWHH) to étalon half-width (HWHH).

atmosphere at range R with thickness ΔR can be derived from Ref. 27 as

$$N_i(R) = \frac{E_0 \lambda}{hc} \frac{A}{R^2} \tau_i \eta_i (\beta_A + \beta_R) \times \Delta R \exp\left[-2 \int_0^R \gamma(\nu) dx\right], \quad (20)$$

where A is the area of the lidar receiver, τ_i and η_i are the transmission and quantum efficiency of the ith channel, respectively, β_A and β_R are the aerosol and Rayleigh backscatter coefficients of the atmosphere per unit solid angle per unit length, respectively, and $\gamma(\nu)$ is the attenuation coefficient of the atmosphere as a result of the combined aerosol and molecular scattering and absorption effects. We note that Eq. (20) is valid for lidar pulse lengths $c\Delta t$, which are much less than the thickness of the layer ΔR.

B. High-Resolution Étalon

We consider first the case of utilizing a high-resolution étalon to sense the Doppler shift of the backscattered aerosol signal for a narrow-band laser. Two narrow-band pulsed solid-state lasers with the potential for making this measurement are injection-seeded Nd:YAG or alexandrite. The Nd:YAG laser could be utilized at either the fundamental at 1.06 μm or the second harmonic at 0.53 μm. Alexandrite operates near 0.76 μm and can be tuned over ±40 nm. For a plane-parallel étalon with an air gap of 5 cm and a finesse of 30 the half-width α is 0.00167 cm^{-1} and the resolving power is 2.8×10^6 at 1.06 μm. For this étalon at 1.06 μm the fractional change in transmittance for a 1-m/s velocity is found from Eq. (19) to be 3.8% at the half-width. The same sensitivity could also be obtained at 0.53 or 0.76 μm by decreasing the étalon gap (or finesse) by the ratio of the wavelengths to maintain a constant resolving power.

We have conducted simulations of the system performance for a lidar, using the edge technique and narrow-band étalons with a resolving power of 2.8×10^6 at wavelengths of 0.53 and 1.06 μm. The transmitter and receiver parameters are given in the second and third columns of Table 1. The laser energy of 1 J at 1.06 μm is available from an injection-seeded Nd:YAG laser at 10–30-Hz repetition rates. The corresponding energies for this laser at the doubled and tripled frequencies are also shown. The beam splitter, which separates the incident beam into edge filter and energy monitor paths, is chosen to provide equal signal to noise for these paths. The value of the ratio of the reflectance to the transmittance (R/T) of this beam splitter is given in Table 1.

The signals backscattered from the atmosphere for an upward-viewing, ground-based lidar with a zenith angle of 50° are shown in Figs. 4 and 5 for wavelengths of 1.06 and 0.53 μm, respectively. The simulations are for the clear air aerosol model of McClatchey *et al.*[28] for a mid-latitude summer atmosphere. The aerosol and Rayleigh components of the backscattered signal measured by both the étalon and energy monitor detectors are shown. The outgoing laser frequency is located at the half-width of the étalon fringe where the sensitivity is a maximum. Since the spectral width of the Rayleigh return is more than an order of magnitude larger than the width of the high-resolution étalon fringe, the spectral distribution of the Rayleigh return is nearly constant over the bandpass of the étalon. The Rayleigh signal transmitted by the étalon is thus only weakly dependent on the Doppler shift and is essentially a background term. If this term is treated as independent of the Doppler shift, it contributes a maximum velocity error of 0.125–0.25 m/s for a wind velocity of 25 m/s. An iterative correction procedure would reduce this error to < 0.01 m/s.

An accurate determination of the differential normalized signal requires that the aerosol measurement be corrected for the Rayleigh background. This can be accomplished by using the signal reflected from the high-resolution étalon in a manner that is

Table I. Lidar System Parameters Used in the Simulations

Wavelength (nm)	1064	532	355
Energy (J)	1.0	0.55	0.28
Zenith angle (deg)	50	50	50
Receiver area (m^2)	0.166	0.166	0.166
Optical efficiency[a]	0.8	0.8	0.8
Laser FWHH (cm^{-1})	0.001	0.002	0.004
Étalon HWHH (cm^{-1})	0.00167	0.00333	0.042
Detector type	APD[b]	PMT[c]	PMT
Quantum efficiency	0.4	0.2	0.3
Beams splitter R/T	40/60	60/40	15/85

[a]This does not include the transmission of the edge filter or the transmission or reflection of the final beam splitter.
[b]Avalanche photodiode.
[c]Photomultiplier tube.

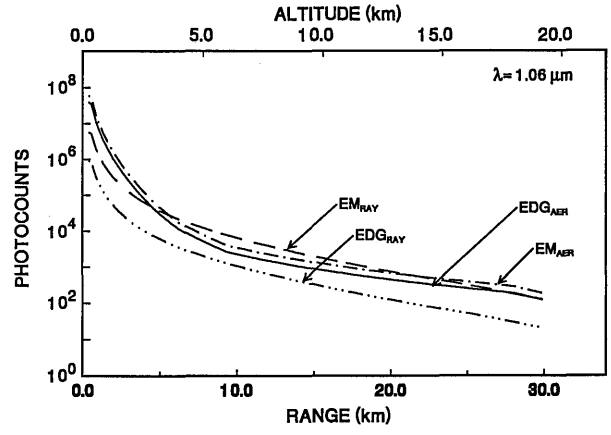

Fig. 4. Simulations of the detected photocounts for the signal backscattered from the atmosphere for an upward-viewing, ground-based lidar at 1.06 μm with a 50-deg zenith angle. The aerosol and Rayleigh (AER and RAY) components of the edge and energy monitor (EDG and EM) signals are shown as a function of altitude (range). The results are for a single shot for a vertical resolution of 100 m, a 0.5-m-diameter telescope, a laser energy of 1 J, and an étalon with a half-width of 0.00167 cm^{-1} (see Table 1).

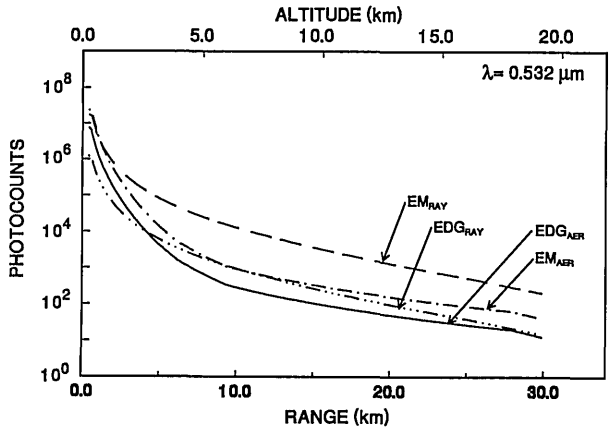

Fig. 5. Simulations of the detected photocounts for the signal backscattered from the atmosphere for an upward-viewing, ground-based lidar at 0.532 μm with a 50-deg zenith angle. The aerosol and Rayleigh (AER and RAY) components of the edge and energy monitor (EDG and EM) signals are shown as a function of altitude (range). Results are for a single shot for a vertical resolution of 100 m, a 0.5-m-diameter telescope, a laser energy of 0.55 J, and an étalon with a half-width of 0.00333 cm^{-1} (see Table 1).

similar to that described by Shipley *et al.*[29] The signal reflected from the étalon is the complement of the transmitted signal and thus contains a large fraction of the Rayleigh signal as well as an aerosol component. A second étalon is introduced in the reflected beam to eliminate the aerosol component. With a knowledge of the spectral response of the two étalons and an estimate of the Rayleigh width, the magnitude of the Rayleigh background can be determined. The aerosol signal for the edge and energy monitor detector channels may then be determined by subtracting the corresponding Rayleigh component from each of the above detector signals. We note that the second étalon, which is centered on the laser frequency, is broad with respect to the edge étalon. Thus small changes in the laser frequency introduce only small effects.

The velocity error is found from the sensitivity, which was discussed above, and the signal-to-noise ratio of the atmospheric measurement. We assume that shot noise is the dominant noise source in the following development. A dark noise term is included that is important for low-signal level operation of avalanche photodiodes at 1.06 μm. For the edge channel detector the aerosol component of the return is the signal, and the background is the bandpassed Rayleigh return and the detector dark current. The signal to noise for the edge channel can be derived from Kingston[30] as

$$(S/N)_1^2 = \frac{gF\phi_A}{1 + \frac{M\phi_R}{F\phi_A} + \frac{\psi}{gF\phi_A}}, \qquad (21)$$

where ϕ_A and ϕ_R are the number of aerosol and Rayleigh photons that are incident on the system, respectively, F and M are the fractions of the aerosol and Rayleigh signals transmitted by the étalon, g is the detector quantum efficiency times the optical transmission for all elements other than the étalon, and ψ is the dark current during the observation time Δt, i.e., the internal noise expressed by the equivalent number of photoelectrons emitted at the photocathode in time Δt. For the energy monitor channel detector the signal is the aerosol component of the return and the background is the sum of the Rayleigh return and the detector dark current. The corresponding signal-to-noise term for the energy monitor channel is

$$(S/N)_2^2 = \frac{g_0\phi_A}{1 + \frac{\phi_R}{\phi_A} + \frac{\psi_0}{g_0\phi_A}}, \qquad (22)$$

where g_0 is the detector quantum efficiency times the optical transmission and ψ_0 is the dark noise current during the observation time for the energy monitor detector. The composite signal to noise for the atmospheric measurement is given by Eq. (17) with the signal-to-noise terms of Eqs. (21) and (22).

The horizontal wind error for a measurement is given by Eq. (16b). The signal and background terms needed for the signal-to-noise determination are shown in Figs. 4 and 5. The error in the horizontal component of the wind is shown as a function of altitude in Figs. 6 and 7 for wavelengths of 1.06 and 0.53 μm, respectively. The velocity errors are shown for measurements with the outgoing laser frequency located on the edge at 0.5, 1.0, and 2.0 étalon half-widths from the center of the étalon fringe.

The optimum accuracy is obtained at the half-width, $x = 1$, as expected for a high-resolution laser. A very high accuracy is obtained at 1.06 μm. For a 100-m vertical resolution and a 100-shot average an

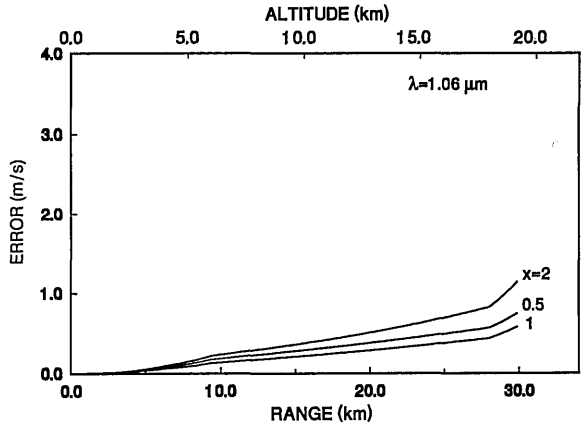

Fig. 6. Simulated errors in the horizontal velocity component of the wind as a function of altitude (range) at 1.06 μm for measurements with the outgoing laser frequency at $x = 0.5$, 1.0, and 2.0 étalon half-widths on the edge of the étalon fringe. Results are for a 100-shot average, a vertical resolution of 100 m, a 0.5-m-diameter telescope, a laser energy of 1 J, and an étalon with a half-width of 0.00167 cm^{-1} (see Table 1).

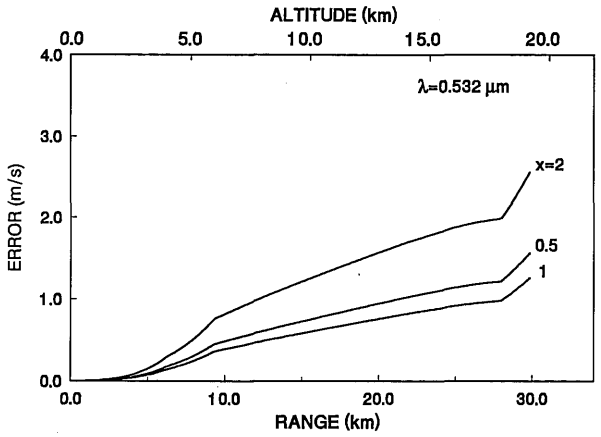

Fig. 7. Simulated errors in the horizontal velocity component of the wind as a function of altitude (range) at 0.532 μm for measurements with the outgoing laser frequency at $x = 0.5$, 1.0, and 2.0 étalon half-widths on the edge of the étalon fringe. Results are for a 250-shot average, a vertical resolution of 100 m, a 0.5-m-diameter telescope, a laser energy of 0.55 J, and an étalon with a half-width of 0.00333 cm^{-1} (see Table 1).

accuracy of better than 0.5 m/s is obtained from the ground to an altitude of 20 km. At 0.53 μm an accuracy of better than 1.25 m/s is obtained for the same altitude range and vertical resolution by averaging 250 shots.

For studies of winds in the lower troposphere an even higher vertical resolution can be obtained. Figure 8 shows the error in the horizontal component of the wind for an altitude range of 0 to 5 km at a wavelength of 1.06 μm. As above the errors are shown for measurements with the outgoing laser frequency located on the edge at 0.5, 1.0, and 2.0 étalon half-widths from the center of the étalon fringe. For a 20-m vertical resolution and a 10-shot average an accuracy of better than 0.5 m/s is obtained

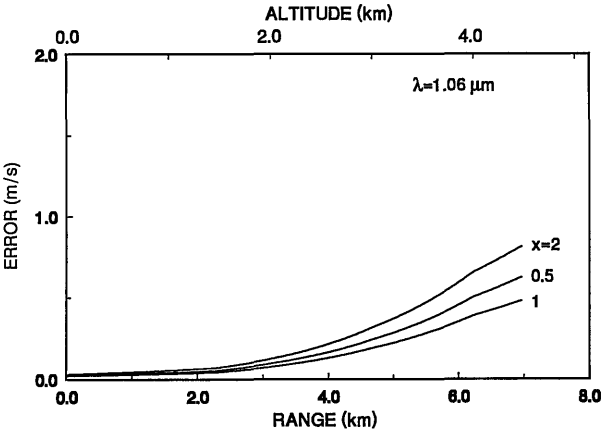

Fig. 8. Simulated errors in the horizontal velocity component of the wind as a function of altitude (range) at 1.06 μm for measurements with the outgoing laser frequency at $x = 0.5$, 1.0, and 2.0 étalon half-widths on the edge of the étalon fringe. Results are for a 10-shot average, a vertical resolution of 20 m, a 0.5-m-diameter telescope, a laser energy of 1 J, and an étalon with a half-width of 0.00167 cm^{-1} (see Table 1).

from 0 to 5 km. Furthermore, in the first 2 km an accuracy of better than 0.2 m/s is obtained with a 20-m vertical resolution. This provides the capability of observing vertical winds directly with high spatial resolution, which permits studies of turbulent motion and the evolution of convective cells in the boundary layer.

We note that for very high accuracy levels, such as are indicated in the simulations for lower tropospheric measurements, the effects of error sources such as velocity turbulence and speckle may become significant. Velocity turbulence within a range cell slightly broadens the spectral distribution of the backscattered laser return. This should not affect the velocity measurement significantly since the edge technique is largely insensitive to the laser spectral characteristics, as was discussed in some detail [see Eqs. (11) and (12)]. For systems employing incoherent detection the effects of speckle can be reduced significantly if a large number of spatial cells are averaged.[31] The number of spatial cells is determined by the field of view of the telescope. For the examples we have considered where a high-resolution Fabry–Perot étalon is used, the field of view of the telescope is determined by the field of view of the étalon[32] and the requirement for matching the throughput ($A d\Omega$) of the telescope to that of the étalon. For a plane étalon with 10-cm-diameter plates and the parameters of Table 1 the telescope field of view is 0.34 mrad, which is ~65 times diffraction limited at 1.06 μm. The number of spatial cells averaged for 10 shots is 4.22×10^4. For a 20-m range element (132-ns integration time) and a laser pulse length of 15 ns the number of independent cells is increased further by a factor of 9 to 3.8×10^5, which limits the signal to noise to 615 and the accuracy to 0.03–0.07 m/s.

C. Low-Resolution Étalon

We consider next a lidar system that determines the average drift velocity of molecules in the atmosphere, i.e., the wind, by measuring the Doppler shift of the thermally broadened molecular backscattered laser signal. The molecular backscattered laser signal is spectrally broadened as a result of Doppler shifts from the random thermal motion of air molecules, Rayleigh scattering, and Brillouin scattering,[32] which introduces two components shifted symmetrically about the peak. The Brillouin scattering effect on the edge filter measurement is small and is not treated quantitatively here. The spectral distribution of the Rayleigh backscattered signal is Gaussian with a width that is proportional to the mean velocity of the molecules. As a result of the two-way path the backscattered signal is double Doppler broadened [see Eq. (13)]. A Fabry–Perot étalon whose fringe width (HWHH) is of the order of or larger than the width of the molecular return (HWHH) is utilized as the edge filter for this measurement. The resolution of this étalon is significantly lower than that of the étalon

considered above. The decreased sensitivity of this system is offset in part by the relativly large molecular signal that is available at UV wavelengths. A frequency-tripled Nd:YAG laser at 355 nm or a XeCl laser at 308 nm is appropriate for this measurement.

At 355 nm the Rayleigh half-width is 0.063 cm^{-1} for a temperature of 280 K. An étalon with an air gap of 0.2 cm and a finesse of 20 would have a fringe of this width. The sensitivity of various étalons is shown in Fig. 9 as a function of the location of the measurement on the edge in units of fringe half-widths. Curves are given for étalon fringe half-widths that are both finer and broader than the Rayleigh half-width. As shown, the general trend is for the peak value of the sensitivity to increase as the étalon resolution increases (the half-width decreases). However, the number of half-widths corresponding to that peak value also increases, which in turn leads to much lower values of transmission [see Eq. (18)]. The effect of the Rayleigh profile on the measurement must also be considered when the étalon width is selected. In Section 2 the edge measurement is shown to be insensitive to the laser width and shape if the edge function is linear over the laser width. In an analogous manner the edge measurement is insensitive to the Rayleigh width and shape if the edge function is linear over the Rayleigh width. Thus, if the étalon width is comparable with or larger than the Rayleigh width, the measurement is desensitized to the detailed spectral properties of the signal, which includes the effects of Rayleigh, aerosol, and Brillouin scattering. However, for an étalon with a width that is much smaller than the Rayleigh width the étalon response is highly nonlinear over the width of the Rayleigh function, and the spectral width and shape of the molecular signal must be known accurately.

The normalized signal determination for the outgoing laser beam utilizes a narrow-band laser, whereas the corresponding measurement for the atmospheric return uses the Rayleigh backscattered signal as described above. For an étalon that has a width of the order of the Rayleigh width, the effect of the Rayleigh width is not negligible. It can be compensated for by correcting the backscattered normalized signal for the effect of Rayleigh broadening. The corrected normalized signal I_{Nc} is

$$I_{Nc} = I_{Nm} \frac{F(\nu)}{F^*(\nu)}, \tag{23}$$

where I_{Nm} is the measured normalized signal, $F(\nu)$ is the convolution of the laser and the edge function, and $F^*(\nu)$ is the convolution of $F(\nu)$ and the Rayleigh spectral distribution. An estimate of the Rayleigh width is the only additional information required to make this correction. Since the Rayleigh width is proportional to the square root of the temperature, the error in this procedure is due to the uncertainty in the temperature of the backscattering layer. The temperature of a given layer generally is known to better than ±5–10 K based on climatic considerations. For an étalon with a width of 0.6–1.5 times the Rayleigh width, the velocity error corresponding to a 5-K temperature error is <0.5 m/s if the location on the edge is chosen to be just short of the peak sensitivity point on the central fringe side of the sensitivity curve (see Fig. 9).

We have conducted simulations for an étalon with a half-width of 0.042 cm^{-1}, an air gap of 0.3 cm, and a finesse of 20 for the case of a tripled Nd:YAG wavelength of 355 nm. The transmitter and receiver parameters are given in the fourth column of Table 1. The Rayleigh and aerosol components of the backscattered signal for both the étalon and energy monitor detectors are shown in Fig. 10 for an upward-viewing, ground-based lidar at 355 nm with a zenith angle of

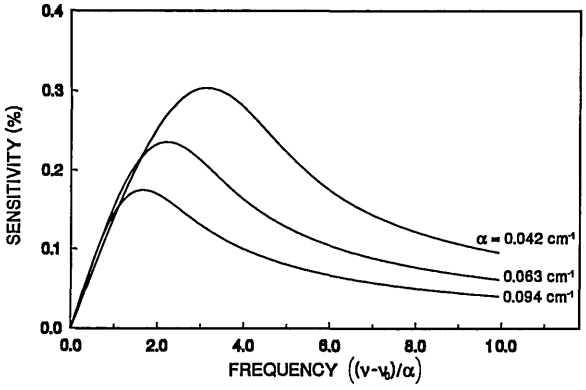

Fig. 9. Sensitivity, the percentage change in the differential normalized edge signal for a velocity of 1 m/s, plotted as a function of the location of the measurement on the edge in units of fringe half-widths. Results are for a wavelength of 0.355 μm for étalon half-widths α that are both finer and broader than the Rayleigh half-width (0.063 cm^{-1}).

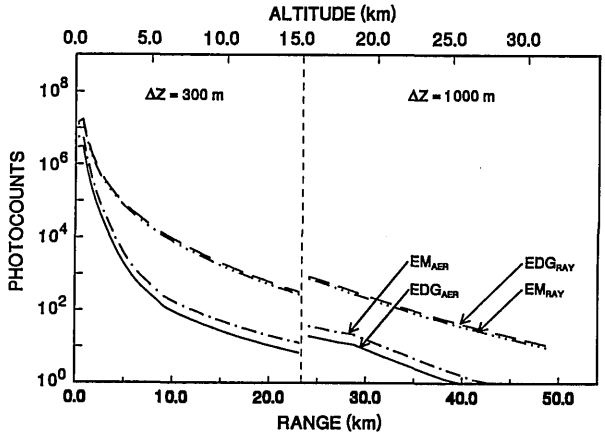

Fig. 10. Simulations of the detected photocounts for the signal backscattered from the atmosphere for an upward-viewing, ground-based lidar at 0.355 μm with a 50-deg zenith angle. The aerosol and Rayleigh (AER and RAY) components of the edge and energy monitor (EDG and EM) signals are shown as a function of altitude (range). Results are for a single shot for a vertical resolution of 300 m (1000 m) for altitudes of <15 km (>15 km), a 0.5-m-diameter telescope, a laser energy of 0.28 J, and an étalon with a half-width of 0.042 cm^{-1} (see Table 1).

50°. The simulations use the same atmospheric and aerosol models as were used above. The laser is located three half-widths out on the edge of the étalon fringe.

The horizontal wind error is determined from Eq. (16b) as before. For both the étalon and energy monitor channels, the signal is the sum of the Rayleigh and aerosol components of the return. The noise is determined by photon fluctuations since the dark current is negligible for high-sensitivity photomultiplier detectors and the signal levels considered here. The signal-to-noise ratio for the étalon channel detector is

$$(S/N)_1^2 = g(F\phi_A + M\phi_R), \tag{24}$$

and M is equal approximately to F for this case. The corresponding signal to noise for the energy monitor channel is

$$(S/N)_2^2 = g_0(\phi_A + \phi_R). \tag{25}$$

The composite signal-to-noise ratio for the atmospheric measurement is found from Eq. (17) with Eqs. (24) and (25). The horizontal wind error is calculated from Eq. (16b) by using the sensitivity for this étalon and the composite signal to noise from above. The error in the horizontal component of the wind is shown in Fig. 11. Errors are shown for measurements with the outgoing laser frequency at two, three, and four étalon half-widths on the edge of the étalon fringe. For altitudes from 0 to 15 km the vertical resolution is 300 m, and 1000 shots are averaged. At higher altitudes the vertical resolution is 1 km, and 5000 shots are averaged. These results for the Rayleigh sensing system may be compared with the velocity errors of the aerosol sensing systems presented in Figs. 6 and 7. As shown in Fig. 11

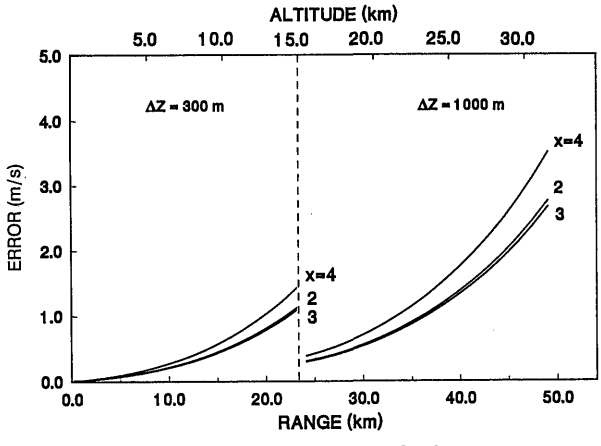

Fig. 11. Simulated errors in the horizontal velocity component of the wind as a function of altitude (range) at 0.355 μm for measurements with the outgoing laser frequency at x = 2.0, 3.0, and 4.0 étalon half-widths on the edge of the étalon fringe. Results are for a 1000 (5000)-shot average, a vertical resolution of 300 m (1000 m) for altitudes of <15 km (>15 km), a 0.5-m-diameter telescope, a laser energy of 0.28 J, and an étalon with a half-width of 0.042 cm^{-1} (see Table 1).

high-accuracy wind measurements with good vertical resolution may be obtained with the Rayleigh edge system by using multiple-shot averaging. We note that the Rayleigh edge technique may be used for wind measurements in the stratosphere as well as in the troposphere, since the molecular backscatter is a reliable source of signal at all altitudes.

4. Conclusions

We have described the edge technique, a powerful new method for the detection and measurement of small frequency shifts. It can be used with a lidar to obtain range-resolved measurements of the wind in the atmosphere with high accuracy and high vertical resolution. With the edge technique the laser frequency is located on the edge of the spectral response function of a high-resolution filter. As a result of the steep slope of the edge, small frequency shifts produce large changes in filter transmission. The Doppler shift is determined from a differential measurement of the frequency of the outgoing laser pulse and the laser return backscattered from the atmosphere. The frequency measurement is accomplished by taking the ratio of the edge filter and energy monitor detector signals to obtain the normalized edge filter output, i.e., the transmission, for both the outgoing and backscattered laser signals on a per pulse basis. The Doppler shift is then determined from a knowledge of the average slope of the instrument function, the convolution of the edge filter and the laser spectral distributions, in the region of measurement. The wind velocity is then found directly from the Doppler shift.

The use of a differential technique to measure the Doppler shift renders the measurement insensitive to laser frequency jitter and drift. We also show that the edge technique is insensitive to the laser spectral width and shape. In particular, for the case of a measurement where the edge function is linear over the laser width and the region of the Doppler shift, the measurement is independent of the laser spectral width and shape and is equivalent to a measurement with a monochromatic laser.

Various instruments, such as an atomic or molecular absorption line, a spherical or plane Fabry–Perot étalon, a Fizeau étalon, or a grating, can be used to produce a sharp edge filter. The edge technique can be used with a broad range of laser wavelengths. We consider three examples that illustrate the power of the edge technique in a ground-based, upward-viewing lidar experiment. These examples use the central fringe of a Fabry–Perot étalon as the edge filter. The first two examples utilize a Nd:YAG laser at 1.06 and 0.53 μm with a high-resolution étalon to measure the Doppler shift of the aerosol return. Methods of correcting for the broadband Rayleigh background are discussed. For an experiment at 1.06 μm with a 20-m vertical resolution and a 10-shot average, an accuracy of better than 0.2 m/s is obtained in the first 2 km, and an accuracy of better

than 0.5 m/s is obtained to 5 km with high-performance avalanche photodiode detectors. For a 100-m vertical resolution and a 100-shot average an accuracy of better than 0.5 m/s is obtained from the ground to an altitude of 20 km. A somewhat lower accuracy of 1.25 m/s is obtained at 0.53 μm by averaging 250 shots.

The third example presents a method of determining the wind by measuring the average drift component of the molecular velocity. In this case the Rayleigh return provides the signal used to determine the wind velocity. A laser operating in the UV, such as a tripled Nd:YAG at 355 nm, permits very large signals to be obtained. The power of the edge technique is clearly shown in this example since accuracies of the order of 1 m/s are obtained although the thermal molecular velocities, which give rise to the spectral broadening of the Rayleigh return, are of the order of 300 m/s. For this measurement a lower-resolution étalon with a width that is two thirds of the Rayleigh width is used. For a 300-m vertical resolution and a 1000-shot average, accuracies of better than 1.0 m/s are obtained to an altitude of 15 km. For a 1-km vertical resolution and a 5000-shot average accuracies of better than 2.0 m/s are obtained to an altitude of 30 km. A wind sensing system that uses the Rayleigh return is significant since the Rayleigh backscatter is a reliable source of signal, even for stratospheric measurements.

We are currently developing a lidar system with an expected performance that is similar to that of the simulations in Section 3. This lidar system permits us to use various edge filters to make high-accuracy, high-vertical-resolution wind measurements by using either the aerosol or the Rayleigh backscattered atmospheric signal.

References

1. C. L. Korb and B. M. Gentry, "New Doppler lidar methods for atmospheric wind measurements—the edge technique," in *Conference on Lasers and Electro-Optics,* Vol. 7 of 1990 OSA Technical Digest Series (Optical Society of America, Washington, D.C., 1990), pp. 322–324.
2. R. Atlas, E. Kalnay, and M. Halem, "Impact of satellite temperature sounding and wind data on numerical weather prediction," Opt. Eng. **24,** 341–346 (1985).
3. R. Atlas, E. Kalnay, W. Baker, J. Susskind, D. Reuter, and M. Halem, "Observing system simulation experiments at GSFC," in *Global Wind Measurements,* W. Baker and R. Curran, eds. (Deepak, Hampton, Va., 1985), pp. 65–71.
4. M. Halem and R. Dlouhy, "Observing system simulation experiments related to spaceborne lidar wind profiling. Part I: Forecast impacts of highly idealized observing systems," presented at the American Meteorological Society Conference on Satellite Remote Sensing and Applications, Clearwater, Fla., 1984.
5. J. Bilbro, G. Fichtl, D. Fitzjarrald, M. Krause, and R. Lee, "Airborne Doppler lidar wind field measurements," Bull. Am. Meterol. Soc. **65,** 348–259 (1984).
6. F. F. Hall, Jr., R. M. Huffaker, R. M. Hardesty, M. Jackson, T. R. Lawrence, M. Post, R. Richter, and B. F. Weber, "Wind measurement accuracy of the NOAA pulsed infrared Doppler lidar," Appl. Opt. **23,** 2503–2506 (1983).
7. M. J. Post and R. E. Cupp, "Optimizing a pulsed Doppler lidar," Appl. Opt. **29,** 4145 (1990).
8. R. T. Menzies and R. M. Hardesty, "Coherent Doppler lidar for measurements of wind fields," Proc. IEEE **77,** 449–462 (1989).
9. R. T. Menzies, "Doppler lidar atmospheric wind sensors: a comparative performance evaluation for global measurement applications from Earth orbit," Appl. Opt. **25,** 2546–2552 (1986).
10. J. C. Petheram, J. Shanley, J. Sroga, R. Vitz, A. Wissinger, and T. R. Lawrence, "The laser atmospheric wind sounder—preliminary design," in *Fifth Conference on Coherent Laser Radar: Technology and Applications,* C. Werner and J. Bilbro, eds., Proc. Soc. Photo-Opt. Instrum. Eng. **1181,** 66–78 (1989).
11. R. Curran, ed., *Laser Atmospheric Wind Sounder,* EOS Instrument Panel Report, NASA Earth Observing System Rep. (National Aeronautics and Space Administration, Washington, D.C., 1987), Vol. IIg.
12. W. Baker and R. J. Curran, eds., *Aerosol Measurement Program Strategy for Global Aerosol Backscatter Model Development,* NASA Workshop Rep. STC 2081 (Deepak, Hampton, Va., 1985).
13. T. Kane, B. Zhou, and R. Byer, "Potential for coherent Doppler wind velocity lidar using neodymium lasers," Appl. Opt. **23,** 2477–2481 (1984).
14. T. Kane, W. Kozlovksy, R. Byer, and C. Byvik, "Coherent laser radar at 1.06 μm using Nd:YAG lasers," Opt. Lett. **12,** 239–241 (1987).
15. M. Kavaya, S. Henderson, J. Magee, C. Hale, and R. M. Huffaker, "Remote wind profiling with a solid-state Nd:YAG coherent lidar system," Opt. Lett. **14,** 776–778 (1989).
16. S. W. Henderson, C. P. Hale, J. R. Magee, M. J. Kavaya, and A. V. Huffaker, "Eye-safe coherent laser radar system at 2.1 μm using Tm,Ho:YAG lasers," Opt. Lett. **16,** 773–775 (1991).
17. V. Abreu, "Wind measurements from an orbital platform using a lidar system with incoherent detection: an analysis," Appl. Opt. **18,** 2992–2997 (1979).
18. P. Hays, V. Abreu, J. Sroga, and A. Rosenberg, "Analysis of a 0.5 micron spaceborne wind sensor," presented at the American Meteorological Society Conference on Satellite Remote Sensing and Applications, Clearwater, Fla., 1984.
19. I. McDermid, J. Laudenslager, and D. Rees, "Ultraviolet-excimer laser-based incoherent Doppler lidar system," in *Global Wind Measurements,* W. Baker and R. Curran, eds. (A. Deepak, Hampton, Va., 1985), pp. 149–155.
20. V. J. Abreu, J. Barnes, P. B. Hays, and W. R. Skinner, presented at the Second Symposium on Tropospheric Profiling Needs and Technology, Boulder, Colo., 1991.
21. M. L. Chanin, A. Garnier, A. Hauchecorne, and J. Porteneuve, "A Doppler lidar for measuring winds in the middle atmosphere," Geophys. Res. Lett. **16,** 1273–1276 (1989).
22. B. Gentry and C. L. Korb, "Doppler velocimetry with submeter-per-second accuracy using the edge technique," in *1991 Annual Meeting,* Vol. 17 of 1991 OSA Technical Digest Series (Optical Society of America, Washington, D.C., 1991), pp. 66–67.
23. M. Born and E. Wolf, *Principles of Optics* (Pergamon, London, 1980), Chap. 7, pp. 323–329.
24. G. Hernandez, "Analytical description of a Fabry–Perot photoelectric spectrometer," Appl. Opt. **5,** 1745–1748 (1967).
25. F. Bayer-Helms, "Analyse von Linienprofilen. I. Grundlagen und Messeinrichtungen," Z. Angew. Phys. **15,** 330–338 (1963).
26. C. L. Korb, G. K. Schwemmer, M. Dombrowski, and C. Y. Weng, "Airborne and ground based lidar measurements of the atmospheric pressure profile," Appl. Opt. **28,** 3015–3020 (1989).

27. R. T. H. Collis, *Lidar,* vol.. 13 of Advances in Geophysics (Academic, New York, 1969), pp. 113–139.
28. R. A. McClatchey, R. Fenn, J. Selby, F. Volz, and J. Garing, in "Optical properties of the atmosphere," U.S. Air Force Cambridge Research Laboratory, Bedford, Mass., Environmental Research Paper 72-0479 (1972).
29. S. T. Shipley, D. Tracy, E. Eloranta, J. Trauger, J. Sroga, F. Roesler, and J. Weinman, "High spectral resolution lidar to measure optical scattering properties of atmospheric aerosols. 1: Theory and instrumentation," Appl. Opt. **22,** 3716–3732 (1983).
30. R. H. Kingston, *Detection of Optical and Infrared Radiation* (Springer-Verlag, Berlin, 1978).
31. J. W. Goodman, "Statistical properties of laser speckle patterns," in *Laser Speckle and Related Phenomena,* J. C. Dainty, ed. (Springer-Verlag, Berlin, 1975), pp. 9–75.
32. P. Jacquinot, "The luminosity of spectrometers with prisms, gratings, or Fabry–Perot étalons," J. Opt. Soc. Am. **44,** 761–765 (1954).
33. A. T. Young and G. Kattawar, "Rayleigh-scattering line profiles," Appl. Opt. **22,** 3668–3670 (1983).